NOVEL SILICON MICROPARTICLES TO IMPROVE SUNLIGHT STABILITY OF RAW POLYPROPYLENE

O. Gil-Castell[1], J. D. Badia[1,2], R. Teruel-Juanes[1], I. Rodriguez[3], F. Meseguer[3,*], A. Ribes-Greus[1,*].

DOI: http://dx.doi.org/10.1016/j.eurpolymj.2015.06.031

Please, cite as:

O. Gil-Castell, J. D. Badia, R. Teruel-Juanes, I. Rodriguez, F. Meseguer, A. Ribes-Greus. Novel silicon microparticles to improve sunlight stability of raw polypropylene. European Polymer Journal 2015; 70, 247-261

[1]Instituto de Tecnología de los Materiales (ITM), Universidad Politècnica de València (UPV) Camino de Vera s/n, 46022 Valencia, Spain.

[2]Departament d'Enginyeria Química. Escola Tècnica Superior d'Enginyeria, Universitat de València,

Av. de la Universitat s/n, 46100 Burjassot, Spain

[3]Instituto de Tecnología Química (CSIC-UPV)

Av. de los Naranjos s/n, 46022 Valencia, Spain

*Corresponding authors:

F. Meseguer fmese@fis.upv.es

A. Ribes-Greus aribes@ter.upv.es

O. Gil-Castell, J. D. Badia, R. Teruel-Juanes, I. Rodriguez, F. Meseguer, A. Ribes-Greus.
Novel silicon microparticles to improve sunlight stability of raw polypropylene. European Polymer Journal 2015; 70, 247-261

NOVEL SILICON MICROPARTICLES TO IMPROVE SUNLIGHT STABILITY OF RAW POLYPROPYLENE

O. Gil-Castell[1], J. D. Badia[1,2], R. Teruel-Juanes[1], I. Rodriguez[3], F. Meseguer[3,*], A. Ribes-Greus[1,*].

Abstract

Oxidation of polyolefins by ultraviolet/visible irradiation is a significant limitation for their use in several technological applications. The use of high-tech additives such as silicon microparticles becomes a compositing strategy that can improve the performance of these materials at long-term service conditions. Silicon particles were added to non-additivated raw polypropylene (PP) prepared by hot melt extrusion and subjected to accelerated sunlight irradiation tests. The stability of thermal properties, mechanical performance and thermal decomposition behaviour of composites was evaluated by differential scanning calorimetry, dynamic mechanical-thermal analysis and thermogravimetry. This paper shows the potential of silicon microparticles to protect PP from degradation during both processing and accelerated sunlight irradiation. The addition of polydisperse silicon microparticles to the raw polypropylene preserved the appearance and improved the thermal behaviour, mechanical properties and thermal stability. It was found that silicon particles at 5 wt% provided a suitable protection of raw non-additivated PP against sunlight irradiation.

Graphical abstract

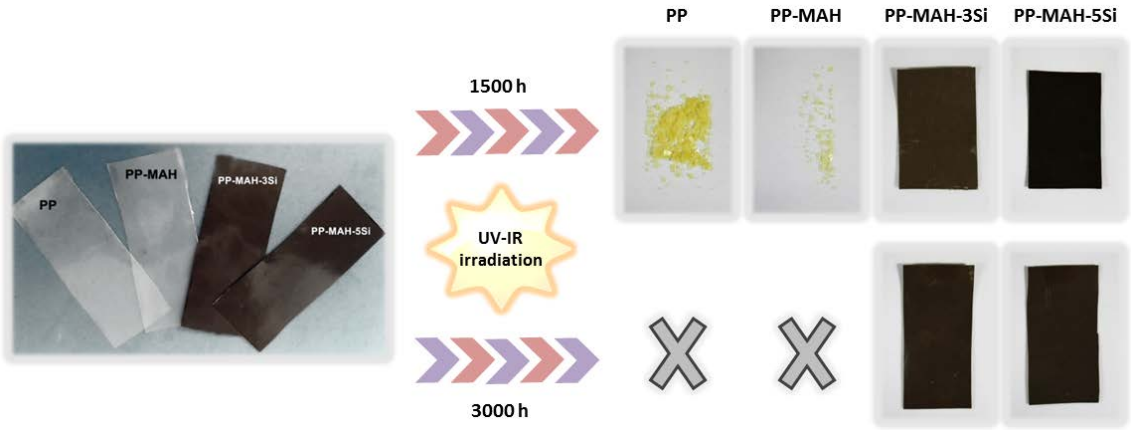

Keywords

Silicon microparticles, polypropylene, polyolefin, composite, sunlight irradiation, photo-degradation, thermal analysis, plastic additives, near-IR reflective pigment

1. Introduction

Polypropylene (PP) is one of the most extensively used polymers in several industrial sectors due to its attractive properties such as suitable processability, feasible mechanical properties, low price and low weight, among others [1]. Wiring, construction, automotive and packaging are some of the main areas. Therefore, the stabilization against different factors which cause polymer degradation such as UV-radiation, temperature, stress loading, water absorption and weathering, among others, is considered crucial for long-term applications.

It is well known that the main effects of photo-oxidation of polypropylene consist in the reduction in molecular size, crystallisation and formation of extra chemical groups, as hydroperoxides and carbonyl species such as ketones, esters and acids [2] [3] [4] [5] [6]. Several protective measures have been thus proposed to increase stability against sunlight irradiation and different kinds of additives have been considered.

Hindered amine light stabilizers (HALS) were introduced more than 25 years ago and they led to considerable improvement of polyolefin light stability based on radical scavenging in which nitroxides play a key role reacting with alkyl radicals and forming amino ether, but some drawbacks have been also observed [7] [8] [9]. The basic nature of HALS causes that some acidic substances have a large negative effect on its effectivity. Thus, high temperatures along with HCl, HBr or HNO_3 and, in general, acid rain which are present in the atmosphere of developed countries due to pollution may deactivate the protective capability of HALS [10].

UV-absorbers used solely or in combination with other light stabilizers are considered other group of additives to prevent photo-degradation. Combinations with nickel derivatives were used, especially for the stabilization of polyethylene films applied in agriculture and horticulture [11]. These substances absorb the harmful UV light more effectively than the polymer and can transform the excess of energy as heat or less-harmful radiation. A main disadvantage of UV absorbers, however, is the necessity of certain sample thickness that permits a proper absorption depth [9] [12] [13]. Moreover, as well as described below for HALS, UV absorbers possess an intrinsic durability which can turn in a considerable drawback. Sun irradiation near-IR reflective pigments, based on light scattering like titanium dioxide, zinc oxide or light absorption as carbon black have been considered to prevent polymers from photo-degradation [14] [15] [16] [17] [18]. Nevertheless, the majority of these systems consist in the addition of nanoparticles, which can provoke toxicity and harmful effects when inhaled or ingested by living organisms [19]. In this line, a novel micro-sized material has been recently developed which can improve significantly resistance to photo-degradation when added to a polymeric matrix in comparison with conventional screeners, preventing from harmful drawbacks. Silicon nano and microparticles obtained either by chemical methods [20] [21] [22] or through milling process [23], block very efficiently sun radiation in the whole UV, visible and infrared regions when coated on a surface. A 20 μm thick coating of silicon microparticles is able to block 99% of the whole sun radiation. This protective mechanism is due to huge value of the refractive index much larger than that for any other material, as titanium dioxide, used for light protection [20].

The aim of the present study concerns determining the capability of the polydisperse silicon microparticles for sunlight protection when added to a non-additivated raw polypropylene matrix. In order to avoid problems derived of phase separation between matrix and particles, some additives acting as coupling agents can be added to the composite. Maleic Anhydride (MAH) grafted PP has been proved to be an effective functional molecule for the reactive coupling

between polypropylene (PP) and other polymers [24] [25] and loadings [26] [27] [28] [29] [30] [31]. Concretely, for silicon microparticles the use of MAH prevented the composites from the phase separation and conglomeration of silicon domains. Moreover, the inclusion of micron-sized particles usually affects polymer properties and behaviour, as crystallisation process, melt processing, thermal stability or mechanical properties, which have to be studied [32] [33] [34] [35]. Therefore, a composite of grafted MAH-PP blended with non-additivated raw PP and silicon microparticles was considered for the study. For this purpose, an initial characterisation of the materials prior to the exposition should be accurately considered. Then, in order to determine how these particles avoid the degradation process, a monitored accelerated sunlight irradiation procedure was carried out.

2. Experimental procedure

2.1 Materials description and sample preparation

Polydisperse silicon microparticles were obtained from metallurgical grade silicon powder (Silgrain® with 99.5% of purity from Elkem), through a process of grinding. Screening of the particles was performed achieving that the 98% were smaller than 2 μm (see **Figure 1**) [23].

Unstabilised isotactic PP ISPLEN PP040 G1E (MFI 3 g/10 min at 230 °C) was supplied by Repsol YPF (Spain) as pellets. Maleic anhydride grafted polypropylene (MAH-PP) from Eastman (Tennessee, USA), coded as G-3003 with a maleic anhydride content of 1%, a molecular weight of 52000 g/mol and a viscosity of 60000 cP (measured at 190°C) was used to ensure coupling of the polypropylene matrix with Si microparticles.

PP, MAH-PP and Si were mixed considering different compositions and resulting specimens were labelled as follows: PP (raw polypropylene), PP-MAH (PP mixed with a 3 wt% of MAH-PP), and PP-MAH-3Si and PP-MAH-5Si (PP-MAH mixed with 3 wt% and 5 wt% of Si, respectively). Mixtures were prepared in a laboratory-scale co-rotating extruder working at 40 rpm and a temperature program of 185-190-195 ºC from feeder to die. Afterwards, 200 μm thick probes were obtained by hot compression moulding at 190 ºC, following a force (kN) – time (min) program of (i) 0-20, (ii) 440-3, (iii) 660-3 and (iv) 880-4, followed by a quenching step to room temperature through water immersion.

2.2 Accelerated sunlight irradiation procedure

Accelerated sunlight irradiation was carried out by exposing the samples to controlled cycles of intense light into an Atlas Suntest XLS+ Xenon Exposure equipment (Illinois, USA) with black panel temperature of 50ºC and irradiance of 600 $J \cdot s^{-1} \cdot m^{-2}$ in the UV-visible range wavelength (λ = 280–800 nm). Several irradiation stages were considered at 250, 750, 1500, 2250 and 3000 h. Even though such testing cannot reproduce all the elements of weathering and exactly predict the performance of these samples in a real outdoor exposure, some meaningful relative comparisons can be done. As a reference, the data at Jacksonville, Florida (USA), with an annual total radiant energy of 5800 $MJ \cdot m^{-2}$ (λ = 280–3000 nm) are considered. According to bibliography [36], this total radiation in the UV-visible range (λ = 280–800 nm) would correspond to 3248 $MJ \cdot m^{-2}$. Thus, the equivalence of 1 hour of simulated irradiation would be equivalent to 5.83 hours of real exposure in Jacksonville, Florida. **Table 1** shows the equivalence for the different stages of irradiation.

Table 1. Approximated real exposure for Jacksonville, Florida (USA) of the considered irradiation stages in the UV-visible wavelength range.

Stage	Simulated exposure (hours)	Approximated real exposure (months)
A	250	2.02
B	750	6.07
C	1500	12.14
D	2250	18.21
E	3000	24.27

2.3 Analytical techniques

Particles morphology and size distribution profile were assessed by Scanning Electron Microscopy (SEM) and Dynamic Light Scattering (DLS) respectively. Thermal properties and stability as well as mechanical properties were characterised by differential scanning calorimetry (DSC), dynamic mechanical-thermal analysis (DMTA) and thermogravimetric analysis (TGA) to study both the effect of the addition on the initial properties of PP and on its durability along exposure to UV-visible irradiation.

2.3.1. Scanning Electron Microscopy (SEM)

Scanning electronic Microscopy images were taken on a Jeol JSM-6300 scanning electronic microscope after a gold sputtering of the samples deposited on SEM mounts. Accelerating voltages of 20 kV were employed.

Composite polymers were cut perpendicularly to the lamellar direction in order to examine particles distribution inside the samples and to obtain a cross section view of the specimens.

2.3.2 Dynamic Light Scattering (DLS)

Particle size distribution profile was obtained by a Mastersizer 2000 (Malvern) based on dynamic light scattering technique.

2.3.3 Differential scanning calorimetry (DSC)

Calorimetric experiments were carried out by means of a Mettler-Toledo DSC 820 series (Columbus, USA), previously calibrated by In and Zn standards. Samples of ~4 mg were analysed between 20 and 200 ºC with a heating/cooling/heating rate of 10 °C·min^{-1} under a nitrogen flow of 50 ml·min^{-1}. The specimens were characterized at least by triplicate and the averages of temperatures and enthalpies were taken as representative values. The melting and crystallisation peak temperatures (T_m, T_c,) were determined from their peaks in thermograms and the enthalpies associated to those events (Δh_m, Δh_c) were determined using constant integration limits. The degree of crystallinity (X_c) was calculated by **Equation 1**.

$$X_c = \frac{1}{(1-m_p)} \frac{\Delta h_m}{\Delta h_{m0}} \times 100 \qquad \textbf{(Equation 1)}$$

where Δh_{m0} is the melting enthalpy for a 100% crystalline PP (207 J·g^{-1} [37]), and $(1 - m_p)$ is the weight fraction of PP. The lamellar thickness distribution was calculated [38] [39] [40] by applying the Thomson-Gibbs equation (**Equation 2**),

$$l_C(T_m) = \left[\left(1 - \frac{T_m}{T_m^0}\right) \cdot \frac{\Delta h_{mV}}{2 \cdot \sigma_e}\right]^{-1} \qquad \textbf{(Equation 2)}$$

where T_m is the melting temperature; T_m^0 is the equilibrium melting temperature of an infinite crystal (187.7 ºC); σ_e is the surface free energy of the basal plane where the chains fold ($49.6 \cdot 10^{-3}$ J·m^{-2}); and Δh_{mV} is the melting enthalpy per volume unit ($1.34 \cdot 10^8$ J·m^{-3}) [41].

2.3.4 Dynamic-mechanic-thermal analysis (DMTA)

Dynamic mechanic thermal analyses were conducted in a small clamping assembly in tension mode, with 5 mm of effective length between clamps, by means of Mettler-Toledo DMA861e (Columbus, USA). The displacement was checked before all the experiments. The deformation force was set at 0.1 N. Experiments at 1 Hz were carried out during heating from 35 to 130 ºC with isothermal steps of 1 ºC. Analyses were performed at least three times per sample to ensure reproducibility.

2.3.5 Thermo-gravimetric analysis (TGA)

Thermal stability was studied by thermogravimetric analysis by means of a Mettler-Toledo TGA 851 series (Columbus, USA). Samples with a mass of 4 mg were introduced in perforated alumina crucibles with capacity of 70 μL, and analysed by a linear heating rate of 10 °C·min^{-1} in the temperature range of 25–800 °C, under a flow rate of 50 mL·min^{-1} of argon. The onset degradation temperature (T_{onset}) was considered as the point in which sample weight decreased 5%. Main peak degradation temperature (T_{peak}) was taken as the minimum of the first-derivative thermogravimetric curve. Experiments were repeated at least three times and the averages were considered as representative values.

3. Results and discussion

The discussion of results is structured in two main sections. Firstly, the effect of the addition of maleic anhydride and Si microparticles to raw PP matrix is reported. Afterwards, the potential of improvement of sunlight protection by Si microparticles for raw PP is considered in terms of mechanical performance and thermal stability.

3.1 Preparation of composites: effect of Si microparticles and MAH coupling agent

3.1.1. Dispersion of Si microparticles

SEM image and particle size distribution profile of the employed silicon microparticles can be seen in **Figure 1a** and **Figure 1b** respectively. The SEM image of the transversal view (**Figure 1c**) as well as a top view optical microscopy image (**Figure 1d**) of the composite PP-MAH-5Si reveal that silicon microparticles are quite well dispersed inside the polymer matrix.

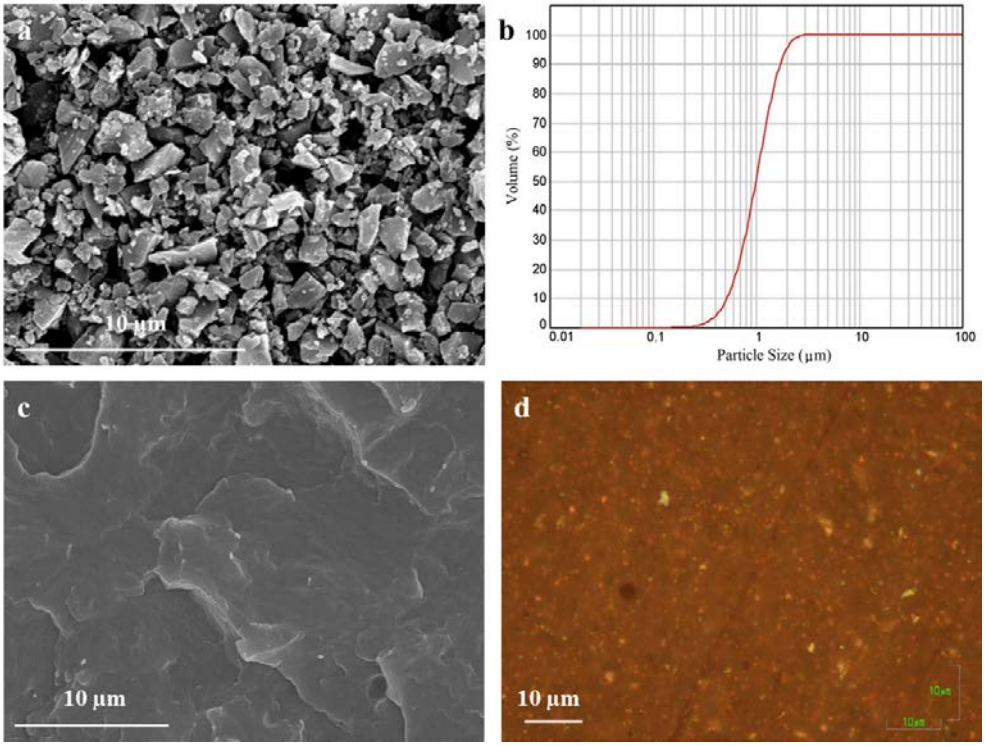

Figure 1: SEM image (a) and size distribution profile (b) of the employed silicon microparticles. SEM cross section view (c) and optical top view image (d) of the composite PP-MAH-5Si.

3.1.2 Morphology and thermal processing windows

Figure 2 shows the thermograms of first heating, cooling, and second heating scans for raw PP, PP-MAH and PP-MAH-Si composites. In general, the addition of a low amount of MAH and the inclusion of Si scarcely modified the crystallisation and melting behaviours of PP. It suggests that the same technological specifications to process PP could be extended to process PP-Si composites.

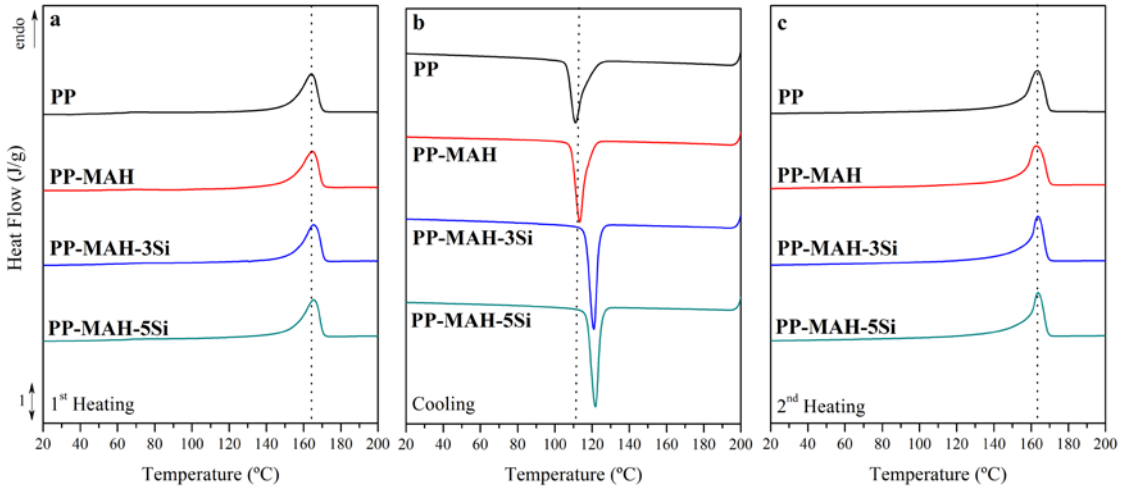

Figure 2. DSC thermograms of 1st heating (a), cooling (b), and 2nd heating scans (c) for raw PP, PP-MAH and PP-MAH-Si composites.

A particular study of the first heating scan (**Figure 2a**) showed that raw PP displayed a single melting peak, characteristic of quenched polypropylene [42] [43]. PP-MAH and PP-MAH-Si

composites displayed the same behaviour: PP-MAH due to the low MAH content and the high molecular weight of the PP [25]; and composites due to the nucleating ability of Si microparticles [44] [45]. Both components tended to co-crystallize and melt in a single peak, at slightly higher temperatures values in the case of composites. **Table 2** shows the peak temperatures, enthalpies and average lamellar thickness obtained from the first heating scan. After quenching procedure, the addition of MAH and Si barely modified the content of crystalline fraction, whereas it promoted the growth of crystals thickness (l_C) (**Figure 3a**). The peak of the distribution increased from ~14.6 for raw PP to ~15.1 nm for PP-MAH, and ~15.6 nm for PP-MAH-3Si and 5Si. Unimodal curves indicated a single population of crystalline domains in each case.

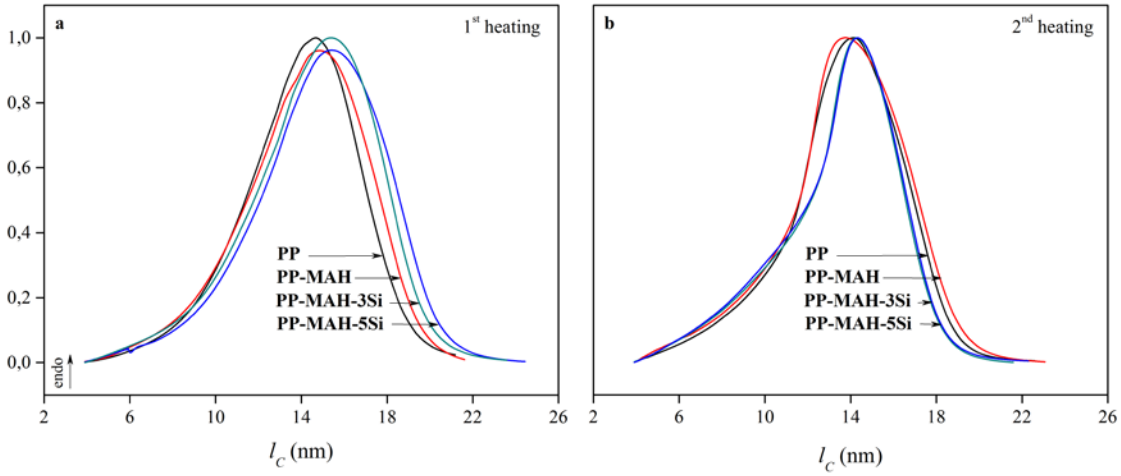

Figure 3. Lamellar thickness distribution for raw PP, PP-MAH and PP-MAH-Si composites in the 1st heating (a) and 2nd heating (b) scans.

Concerning the cooling scan (**Figure 2b**), a single crystallisation peak T_c for all materials is shown. **Figure 8** contains the peak temperatures and enthalpies of this process. The presence of MAH induced an increment of ~1.9% of T_c. A further addition of 3 wt% and 5 wt% of Si gave out an increase of ~6.8% and ~7.5% of T_c, respectively, taking PP-MAH as reference, as reported by other authors [46].

Regarding the second heating scan (**Figure 2c**), similar T_m was found for all materials once the thermal history has been removed. Moreover, Δh_m decreased for composites. Although this lower melting enthalpy is traduced in lower crystalline degree, **Figure 3b** shows that the average l_C remained constant. In addition, it is important to remark that, for composites, the crystalline population was narrowed. **Table 3** shows the peak temperatures, enthalpies and average lamellar thickness for all materials.

3.1.3 Mechanical properties of neat PP-Si composites

Figure 4 shows the storage modulus (*E'*) values that were recorded through dynamic-mechanical thermal analysis at 1 Hz as a function of temperature for PP and composites. According to calorimetric results, the slight nucleating ability of MAH to induce the formation of crystalline fraction was traduced in an increase of ~8% in *E'*. When Si microparticles were added to the coupled PP matrix, *E'* increased ~85% for a 3 wt% of Si and arrived to a ~115% for a 5 wt% of silicon microparticles. Those results were in agreement with other reports combining PP with particles such as zinc oxide [15], clay [26], calcium carbonate [26] [47] or silica [48]. It was remarkable that this increment in modulus was not linked to the crystalline nucleation or growth induced by the presence of Si. Indeed, as shown in the inset of **Figure 4**, similar slopes suggested

that the silicon particles did not affect the profile of viscoelastic behaviour of PP, but just being displaced to higher *E'* values. There was therefore effective stress transfer from the PP matrix to Si particles due to entanglement of the polymer chains with the filler, increasing the stiffness of the segments in the surroundings of the particles [48] [49].

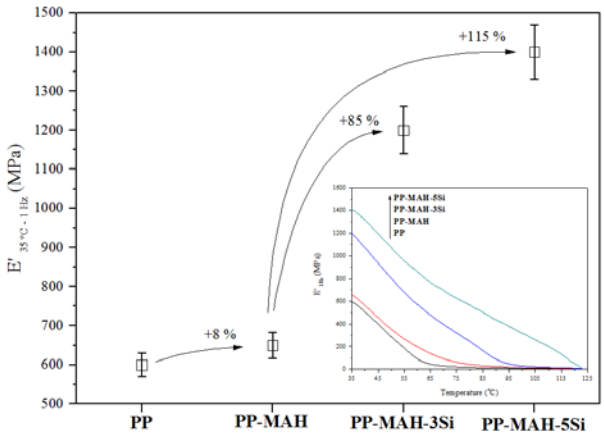

Figure 4. Storage modulus (*E'*) values recorded at 1 Hz and 35 ºC for raw PP, PP-MAH and PP-MAH-Si composites. Inset: Storage modulus (*E'*) profiles recorded at 1 Hz as a function of temperature.

3.1.3 Thermal stability

The thermal stability was assessed by means of thermogravimetric experiments under inert atmosphere. Results are gathered in **Figure 5**, in terms of thermogravimetric and first-derivative thermogravimetric curves (**Figure 5a**), as well as an evolution of peak and onset temperatures (**Figures 5b** and **5c**, respectively). Neither the addition of MAH nor the addition of Si particles modified the mass-loss profile which took place through a single stage. However, the effect of MAH into the PP improved its thermal stability, as shown by slightly higher onset T_{onset} and peak T_{peak} temperature [48]. Due to the addition of Si, a considerable increase in T_{onset} and slight increase in T_{peak} was found, being superior for PP with a 5 wt% of Si. This demonstrated the thermal stabilization by increasing the Si content, as reported using similar particles [33] [50].

As observed in decomposition curve for the composites, silicon microparticles became the remaining residue after combustion of the PP-matrix, remarking the possibility of recovering them at end of life after though a hypothetic energetic valorisation procedure. Thus, this additive can be reused after further purification if necessary, increasing its added-value.

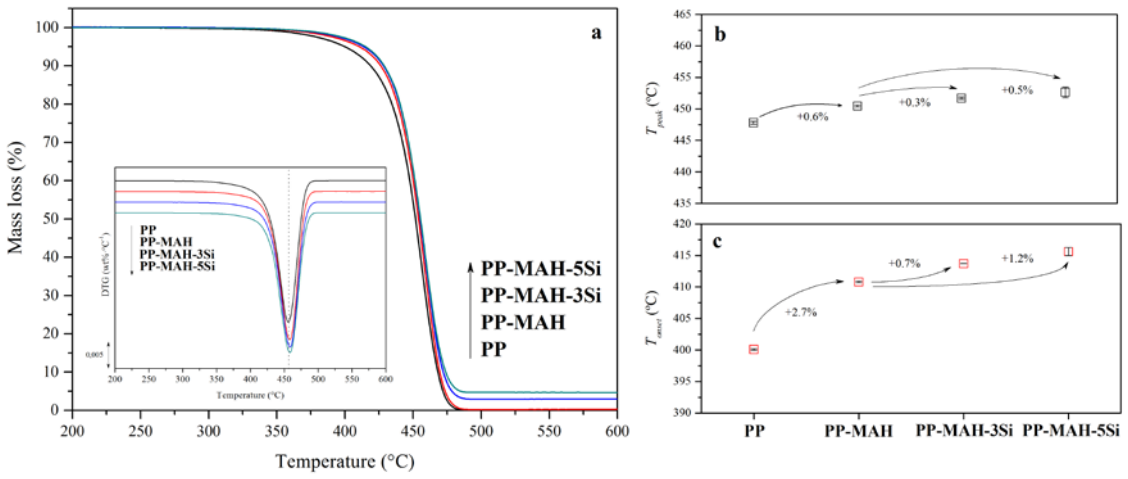

Figure 5. (a) Thermal decomposition profiles and derivative curves, (b) peak decomposition temperature (T_{peak}), and (c) onset degradation temperature (T_{onset}) for raw PP, PP-MAH and PP-MAH-Si composites.

3.2 Durability of composites of PP filled with Si particles under sunlight radiation

Figure 6 shows the appearance of raw PP, PP-MAH and PP-MAH-Si composites after 250, 750, 1500, 2250 and 3000 h of irradiation in the UV-visible wavelength range (λ = 280 – 800 nm). For PP and PP-MAH, samples become semi-opaque after 250 h of irradiation due to the generation of new crystalline domains by chemi-crystallisation [51] [52] [53]. After 750 h, transparent samples turned entirely opaque and whitish. Disintegration took place after 1500 h of irradiation due to the advance of chain scission [15] [54] [55] and the effect of chemi-crystallisation, which is responsible of the surface cracking by contraction of surface layers, causing grave weakening in different properties of the samples after short-term exposures [54] [55].

In contrast, PP-MAH-3Si and PP-MAH-5Si after 250 and 750 h of irradiation showed an apparently similar state than that prior to the exposition. After 1500 h, the sample surface slightly changed, being easily scratched during manipulation, detaching a fine powder. After 2250 h of exposition, the composite films turned slightly brittle and surface appeared to be rougher. Finally, after 3000 h, composites with 3 wt% of Si were delicate to handle and apparently more degraded than those with 5 wt% of Si particles. Thus, a deep study in order to understand the mechanisms and determine the durability of the quality of composites was carried out by thermal analysis [56].

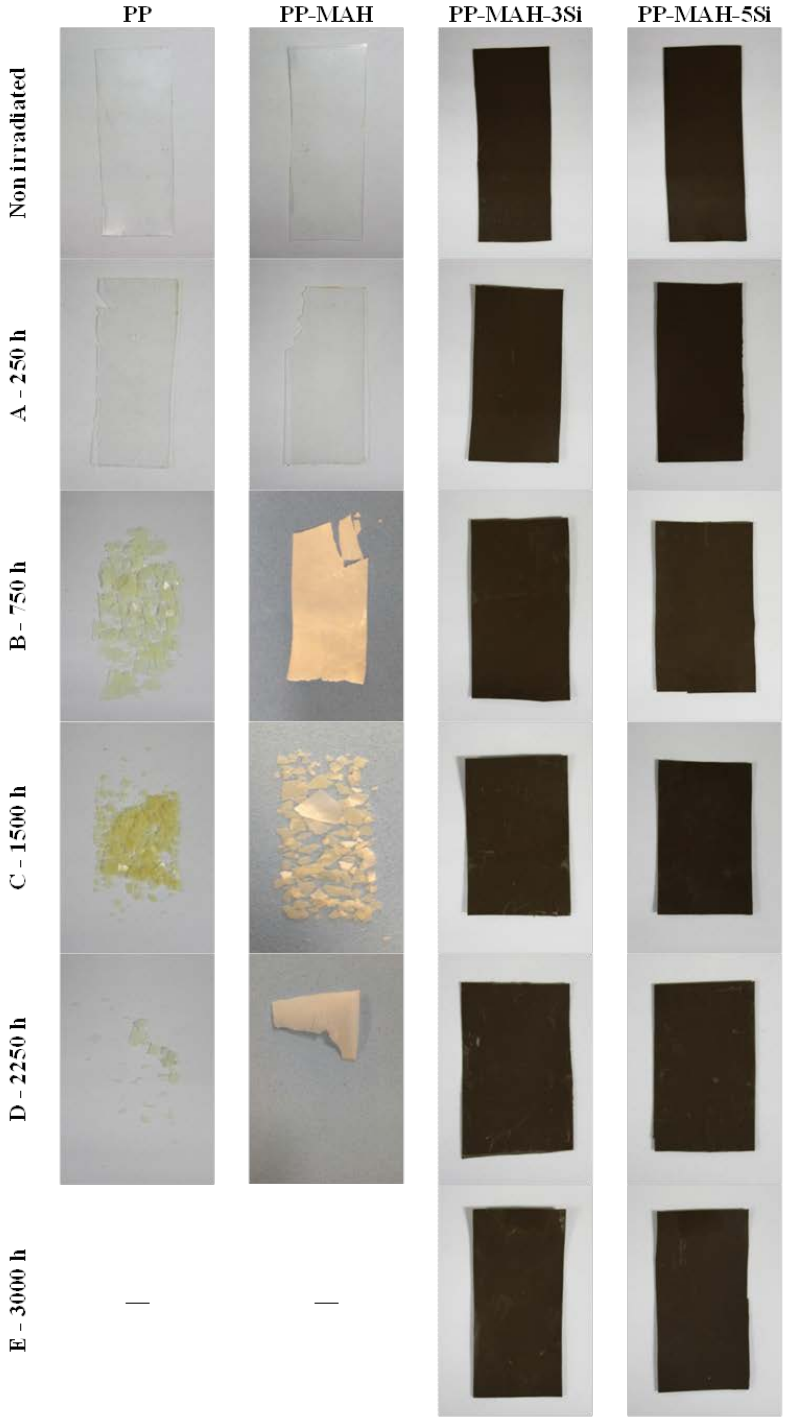

Figure 6. Appearance of raw PP, PP-MAH and PP-MAH-Si composites after 250, 750, 1500, 2250 and 3000 h of irradiation in the UV-visible wavelength range (λ = 280 – 800 nm).

3.2.1 Impact of sunlight radiation on morphology and thermal performance

Figure 7 shows the thermograms of first heating, cooling, and second heating scans for raw PP, PP-MAH and PP-MAH-Si composites after 250, 750, 1500, 2250 and 3000 h of irradiation in the UV-visible wavelength range (λ = 280 – 800 nm) obtained by differential scanning calorimetric analysis (DSC). **Table 2** and **Table 3** show the main temperatures, enthalpies of melting and crystallisation events as well as degree of crystallinity and lamellar thickness values corresponding to the heating scans of the **Figure 7**.

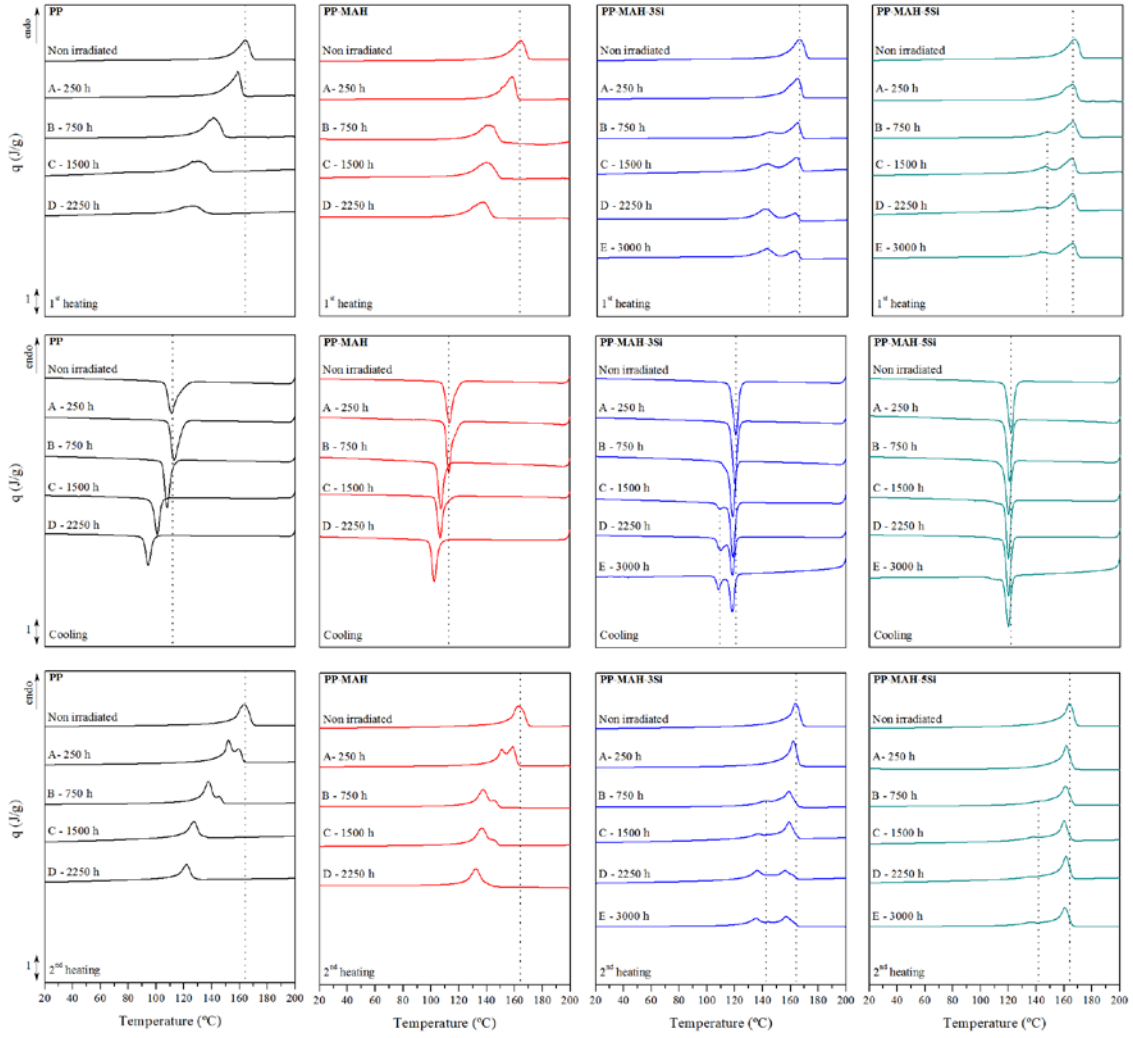

Figure 7. Thermograms of 1st heating, cooling, and 2nd heating scan for raw PP, PP-MAH and PP-MAH-Si composites irradiated in the UV-visible wavelength range (λ = 280 – 800 nm).

In the first heating run, single melting peaks are generally found for PP and PP-MAH. The effect of degradation produced a significant decrease in the melting temperature of the unimodal peak. The addition of silicon particles promoted the apparition of a double-melting behaviour. The original unimodal melting peak remained in the same position, around 165 ºC and a new melting peak appeared after 750 h of irradiation.

Once the effect of thermal history has been removed during the first heating run, the study of the cooling scan indicated that PP and PP-MAH showed a crystallisation peak (T_c) at lower temperatures the higher the exposure to sunlight irradiation was, as shown in **Figure 8a**. This reduction was barely more significant for PP than for PP-MAH. Conversely, the addition of Si

drove the main crystallisation events, giving unaltered T_c. The presence of a 5 wt% of Si prevented the crystallisation of weaker crystalline domains, being the exotherm almost unimodal. Moreover, in **Figure 8b** the evolution of crystallisation enthalpy is represented. As occurred with peak temperature, enthalpy decreased along irradiation for PP and PP-MAH, whereas for PP-MAH-3Si it decreased in last stages of irradiation and for PP-MAH-5Si it remained almost constant. These facts reinforced that irradiation was attacking the amorphous fraction of PP and generated chemical irregularities that difficult the crystallisation process and delayed it [57] [58] [59].

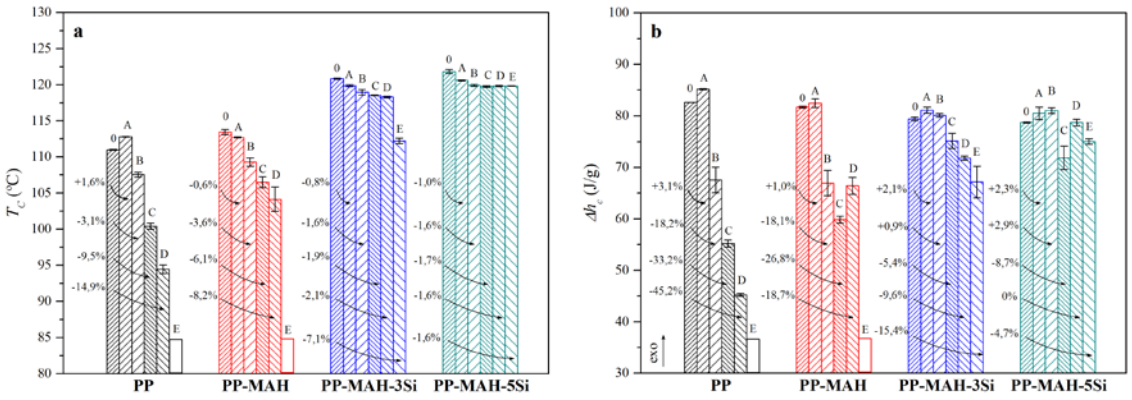

Figure 8. Crystallisation temperature (T_c) (a) and crystallisation enthalpy (Δh_c) (b) for the cooling run for raw PP, PP-MAH and PP-MAH-Si composites irradiated in the UV-visible wavelength range (λ = 280 – 800 nm) (Stages: A = 250 h; B = 750 h; C = 1500 h; D = 2250 h; E = 3000 h).

The study of the second DSC heating run shed light on understanding the bi-modal melting process of materials. Many explanations have been suggested for this phenomenon, such as the presence of different crystalline structures [60] [61]; crystal transformation during heating [62] [63]; reorganisation during heating [43] [64]; or segregation of molecules with low molecular weight which form crystals with lower T_m [65]. A deep study by Rabello and White [57] concluded that degraded molecules form relatively unstable crystals during rapid cooling segment which melt, then re-crystallize into a more stable phase that afterwards melts at a higher temperature, leading to a double melting peak. Indeed, all materials showed a bi-modal melting as a result of a balance of low-T and high-T crystalline populations.

Figure 9 shows that raw PP effectively showed high extent of degradation with a continuous decrease of melting temperatures, moving the balance of initial high-T crystalline populations towards low-T domains [66] [67] [68] [69] [70]. This behaviour also appeared but slightly retarded by the addition of MAH. Concerning the stabilizing effect of Si microparticles, they retained the initial higher lamellar thicknesses around 15 nm, regardless the advance of irradiation, being this influence more relevant for samples loaded with a 5 wt% of Si.

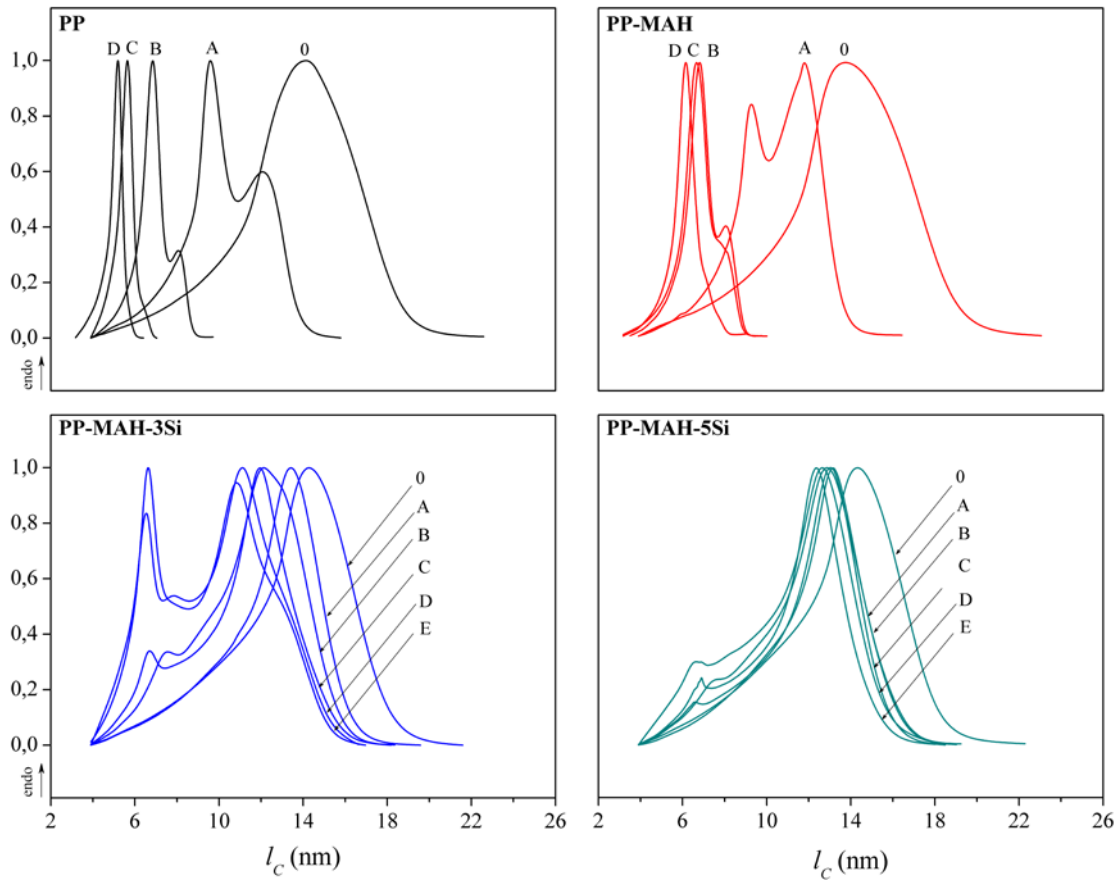

Figure 9. Lamellar thickness distributions for raw PP, PP-MAH and PP-MAH-Si composites in the 2nd heating scan irradiated in the UV-visible wavelength range (λ = 280 – 800 nm) (Stages: A = 250 h; B = 750 h; C = 1500 h; D = 2250 h; E = 3000 h).

Figure 10 plots the evolution of the crystalline degree (X_c) for all materials along the sunlight irradiation tests. Raw PP showed a first increasing X_c tendency with irradiation, ascribed to the chemi-crystallisation of freed segments from chain scission up to 750 h of irradiation [51] [52] [53] [71] [72] [73] [74] [75] [76]. Further exposure provoked a decrease due to massive chain scission. In contrast, PP-MAH did not showed the X_c decrease at longer times of irradiation, thus stabilizing PP due to the chemical bonding of PP and MAH, which let less liable sites for degradation. The addition of Si microparticles hindered chain scission and thus subsequent chemi-crystallisation of low-T crystalline domains, keeping the size of high-T populations, being this effect more relevant with PP loaded with 5 wt% of Si. Therefore the crystalline degree is maintained and even increased regardless the irradiation time.

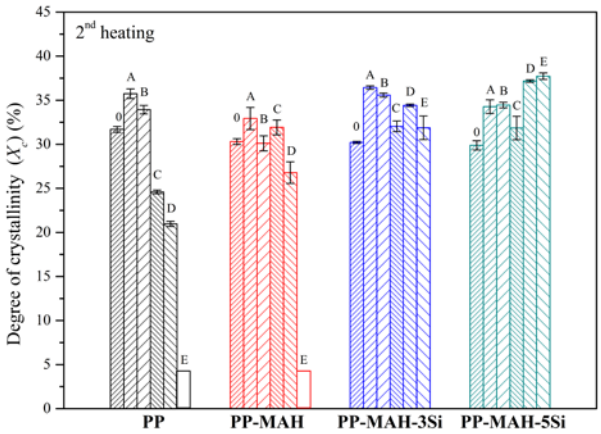

Figure 10. Degree of crystallinity (X_c) for raw PP, PP-MAH and PP-MAH-Si composites irradiated in the UV-visible wavelength range (λ = 280 – 800 nm), as calculated from for the 2nd heating scan (Stages: A = 250 h; B = 750 h; C = 1500 h; D = 2250 h; E = 3000 h).

Si microparticles affected the crystalline fraction, but more than a matter of the effect of irradiation on the degree of crystallinity [77], it was about the distribution of this crystalline phase in the polymer matrix. In fact, a competitive behaviour seems to take place. On the one hand, the natural sunlight degradation profile of PP, which drove the crystalline domains to lower sizes and the stabilizing effect of Si particles, which retains the initial higher lamellar thicknesses around 15 nm, regardless the advance of irradiation. This effect was more relevant for samples loaded with a 5 wt% of Si.

As suggested by Zhao et al. [15], the non-significant variation in X_c for the composites may be due to lower extent of photo-degradation, as a consequence of the effective protection and stabilization function of the Si particles against irradiation, which hindered the chemi-crystallisation phenomenon.

High refractive index microparticles scatter light very efficiently, especially at wavelength values of the order of the particles size [78]. Theory predicts that silicon microparticles can block light up to ten times the size of the particles for wavelength values of the Mie resonances. Although the blocking effect is restricted to a narrow wavelength region, a polydisperse suspension of silicon particles ranging between 0.1 and 2 μm would block very efficiently the whole sun radiation spectrum.

Table 2. Main parameters of calorimetric analysis along the 1st heating scan for raw PP, PP-MAH and PP-MAH-Si composites irradiated in the UV-visible wavelength range (λ = 280 – 800 nm).

1st heating Material	Exposition (stage - hours)	Δh_m ($J \cdot g^{-1}$)	T_m^I (ºC)	T_m^{II} (ºC)	X_c (%)	l_C^I (nm)	l_C^{II} (nm)
PP	0	66.43 ± 0.22	-	163.63 ± 0.64	31.78 ± 0.11	-	12.26 ± 1.82
	A – 250	76.42 ± 1.39	-	158.16 ± 0.68	36.56 ± 0.67	-	11.60 ± 1.83
	B – 750	84.57 ± 0.36	-	141.04 ± 0.18	40.46 ± 0.17	-	7.33 ± 1.82
	C – 1500	59.95 ± 0.48	-	130.08 ± 0.27	28.68 ± 0.23	-	5.93 ± 1.82
	D – 2250	47.13 ± 1.43	-	126.67 ± 0.59	22.55 ± 0.68	-	5.60 ± 1.82
	E – 3000	-	-	-	-	-	-
PP-MAH	0	69.54 ± 1.08	-	164.00 ± 0.93	33.27 ± 0.52	-	14.48 ± 1.83
	A – 250	73.92 ± 1.94	-	157.90 ± 0.29	35.37 ± 0.93	-	11.50 ± 1.83
	B – 750	80.12 ± 0.58	-	142.41 ± 0.00	38.22 ± 0.28	-	7.55 ± 1.82
	C – 1500	81.60 ± 3.02	-	140.49 ± 1.43	39.09 ± 1.44	-	7.24 ± 1.83
	D – 2250	77.76 ± 0.50	-	137.58 ± 0.39	37.21 ± 0.24	-	6.83 ± 1.82
	E – 3000	-	-	-	-	-	-
PP-MAH-3Si	0	62.17 ± 0.09	-	165.03 ± 0.52	29.75 ± 0.04	-	15.15 ± 1.83
	A – 250	66.74 ± 0.34	158.55 ± 1.12	164.58 ± 0.48	31.93 ± 0.16	11.76 ± 1.83	14.85 ± 1.82
	B – 750	73.70 ± 0.92	144.54 ± 0.41	163.86 ± 0.31	35.26 ± 0.44	7.93 ± 1.82	14.39 ± 1.82
	C – 1500	69.38 ± 0.87	142.53 ± 0.08	163.23 ± 0.22	33.20 ± 0.41	7.58 ± 1.82	14.02 ± 1.82
	D – 2250	72.42 ± 0.56	140.65 ± 0.56	162.34 ± 0.06	34.65 ± 0.27	7.27 ± 1.82	13.53 ± 1.82
	E – 3000	70.66 ± 0.70	143.53 ± 1.54	162.23 ± 0.11	33.81 ± 0.33	7.75 ± 1.83	13.47 ± 1.82
PP-MAH-5Si	0	61.83 ± 0.81	-	165.44 ± 0.15	29.58 ± 0.39	-	15.42 ± 1.82
	A – 250	70.71 ± 0.70	159.57 ± 0.00	164.10 ± 0.36	33.83 ± 0.33	12.19 ± 1.82	14.55 ± 1.82
	B – 750	67.40 ± 0.33	145.81 ± 0.40	164.00 ± 0.42	32.25 ± 0.16	8.17 ± 1.82	14.48 ± 1.82
	C – 1500	66.14 ± 2.52	144.42 ± 0.33	163.37 ± 0.16	31.64 ± 1.20	7.91 ± 1.82	14.10 ± 1.82
	D – 2250	68.49 ± 0.31	142.43 ± 0.51	163.91 ± 0.08	32.77 ± 0.15	7.56 ± 1.82	14.43 ± 1.82
	E – 3000	66.83 ± 0.31	133.30 ± 3.65	164.07 ± 0.36	31.98 ± 0.15	8.08 ± 1.83	14.53 ± 1.82

Table 3. Main parameters of calorimetric analysis along the 2nd heating scan for raw PP, PP-MAH and PP-MAH-Si composites irradiated in the UV-visible wavelength range (λ = 280 – 800 nm).

2nd heating Material	Irradiation (stage - hours)	Δh_m (J·g^{-1})	T_m^I (ºC)	T_m^{II} (ºC)	l_C^I (nm)	l_C^{II} (nm)
PP	0	66.23 ± 0.70	-	162.88 ± 0.83	-	13.83 ± 1.83
	A – 250	74.70 ± 1.13	151.72 ± 0.40	159.01 ± 0.44	9.52 ± 1.82	11.95 ± 1.82
	B – 750	70.91 ± 1.03	136.89 ± 1.18	144.19 ± 1.40	9.40 ± 1.83	7.87 ± 1.82
	C – 1500	51.39 ± 0.44	-	127.11 ± 0.18	-	5.64 ± 1.82
	D – 2250	43.83 ± 0.61	-	121.95 ± 0.25	-	5.19 ± 1.82
	E – 3000	-	-	-	-	-
PP-MAH	0	63.35 ± 0.72	-	162.36 ± 0.74	-	13.54 ± 1.83
	A – 250	68.83 ± 2.63	151.29 ± 0.91	158.73 ± 0.77	9.40 ± 1.83	11.84 ± 1.83
	B – 750	62.94 ± 1.77	137.61 ± 0.80	145.50 ± 0.52	6.83 ± 1.83	8.11 ± 1.82
	C – 1500	66.71 ± 1.77	136.54 ± 1.34	144.14 ± 1.49	6.68 ± 1.83	7.85 ± 1.83
	D – 2250	55.99 ± 2.58	-	132.23 ± 1.22	-	6.16 ± 1.83
	E – 3000	-	-	-	-	-
PP-MAH-3Si	0	63.17 ± 0.25	-	163.37 ± 0.43	-	14.1 ± 1.82
	A – 250	76.16 ± 0.39	-	162.26 ± 0.32	-	13.48 ± 1.82
	B – 750	74.39 ± 0.48	142.32 ± 0.28	160.17 ± 0.87	7.54 ± 1.82	12.46 ± 1.83
	C – 1500	66.96 ± 1.26	136.54 ± 0.58	159.04 ± 0.10	6.69 ± 1.82	11.96 ± 1.82
	D – 2250	71.96 ± 0.27	136.07 ± 0.14	156.07 ± 0.19	6.62 ± 1.82	10.83 ± 1.82
	E – 3000	66.60 ± 2.81	132.66 ± 2.54	159.56 ± 2.48	6.21 ± 1.84	12.18 ± 1.84
PP-MAH-5Si	0	62.45 ± 1.10	-	163.56 ± 0.29	-	14.22 ± 1.82
	A – 250	71.63 ± 1.63	-	161.67 ± 0.23	-	13.18 ± 1.82
	B – 750	72.01 ± 0.66	142.34 ± 0.09	161.01 ± 0.49	7.54 ± 1.82	12.85 ± 1.82
	C – 1500	66.58 ± 2.78	137.94 ± 0.16	160.00 ± 0.16	6.87 ± 1.82	12.38 ± 1.82
	D – 2250	77.71 ± 0.30	135.93 ± 0.17	161.38 ± 0.07	6.60 ± 1.82	13.03 ± 1.82
	E – 3000	78.87 ± 0.77	136.28 ± 0.61	162.41 ± 0.25	6.65 ± 1.82	13.57 ± 1.82

3.2.2 Improvement of storage modulus

Figure 11 shows the storage modulus (*E'*) values recorded at 35 ºC from DMTA analyses at 1 Hz for irradiated raw PP, PP-MAH and PP-MAH-Si composites. Due to effect of irradiation, the storage modulus could not be measured in PP and PP-MAH owing to the brittleness and the reduced thickness of the samples. In contrast, composites loaded with a 3 wt% and 5 wt% of Si particles showed similar profiles of reduction of *E'*. Degradation is supposed to have affected the polymer matrix due to sunlight irradiation, but mechanical stresses were supported by the presence of Si in their compositions. In particular, the addition of 5 wt% of Si permitted to obtain significantly high *E'* values after 3000 h of irradiation, at higher levels than those shown by the composites with a 3 wt% of Si.

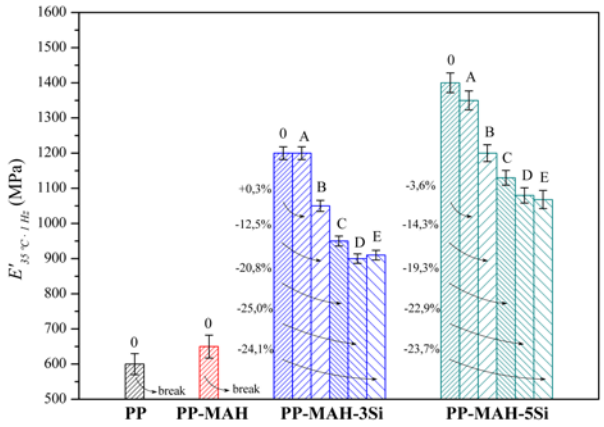

Figure 11. Storage modulus (*E'*) values recorded at 35 ºC and 1 Hz for raw PP, PP-MAH and PP-MAH-Si composites irradiated in the UV-visible wavelength range (λ = 280 – 800 nm) (Stages: A = 250 h; B = 750 h; C = 1500 h; D = 2250 h; E = 3000 h).

3.2.3 Thermal decomposition behaviour

Thermograms of thermal decomposition along with their first-derivative curves are shown in **Figure 12** for irradiated raw PP, PP-MAH and PP-MAH-Si composites. **Figure 13** displays the evolution of their thermal decomposition onset (T_{onset}) (**Figure 13a**) and peak (T_{peak}) temperatures (**Figure 13b)** along irradiation. Despite T_{peak} is usually taken as indicator of degradation, the use of T_{onset} is more sensible and it provides results at a technological context [79] [80] [81]. The initial decomposition process, which consumed around a 10-20% of mass, was enough to trigger the main decomposition process, which was widened in temperature the longer the irradiation was [15]. The most irradiated raw PP started decomposition at temperature immediately above the melting process (~165 ºC), due to the weakened structure. The addition of MAH had no stabilizing effect at this stage and similar profiles than those shown by raw PP were found, even showing fairly similar percentages of reduction in onset and peak temperatures. In contrast, the addition of Si retarded the starting of the first decomposition process, thus preventing the main decomposition up to 750 h of exposition for the case of a 3 wt% of Si and keeping the onset of decomposition within a range of control of ~12.5% up to 3000 h of exposition for the case of a 5 wt% of Si. Thus, the effectiveness of Si particles to stabilize PP along irradiation was shown.

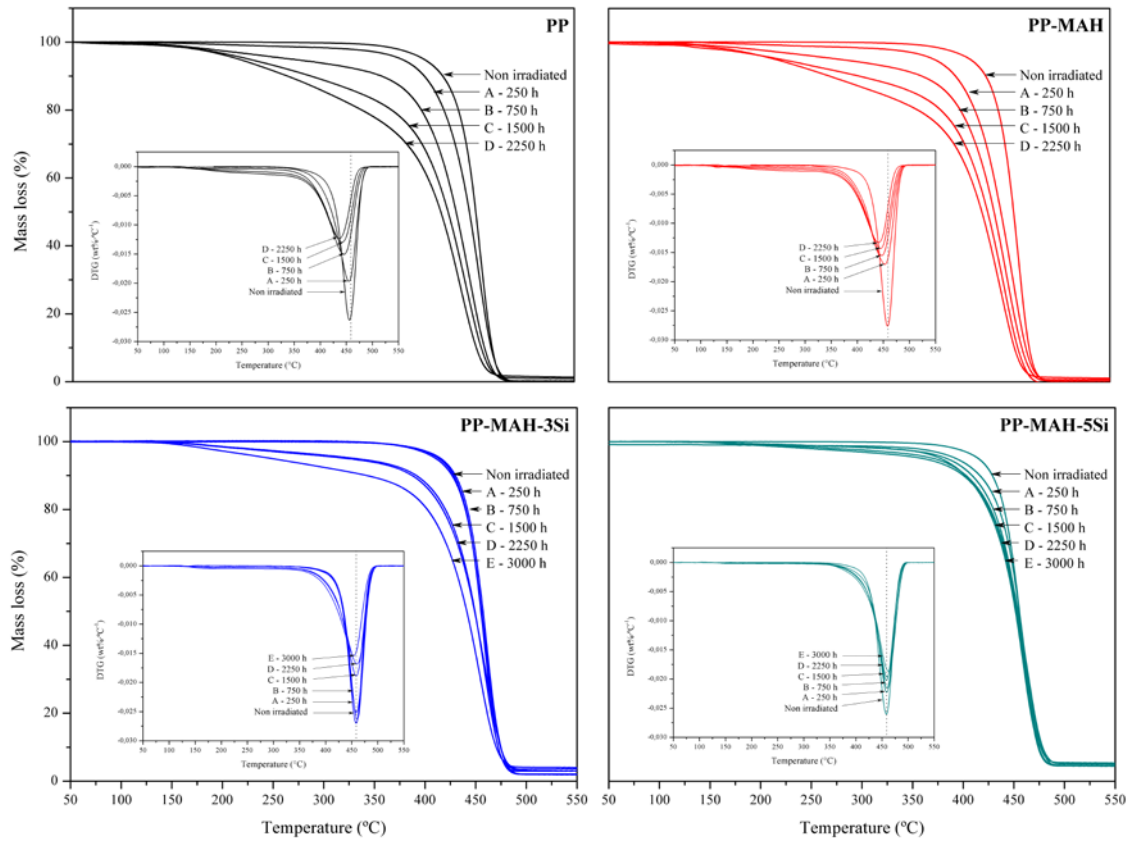

Figure 12. Thermal decomposition profiles and derivative curves (inserted) for raw PP, PP-MAH and PP-MAH-Si composites irradiated in the UV-visible wavelength range (λ = 280 – 800 nm).

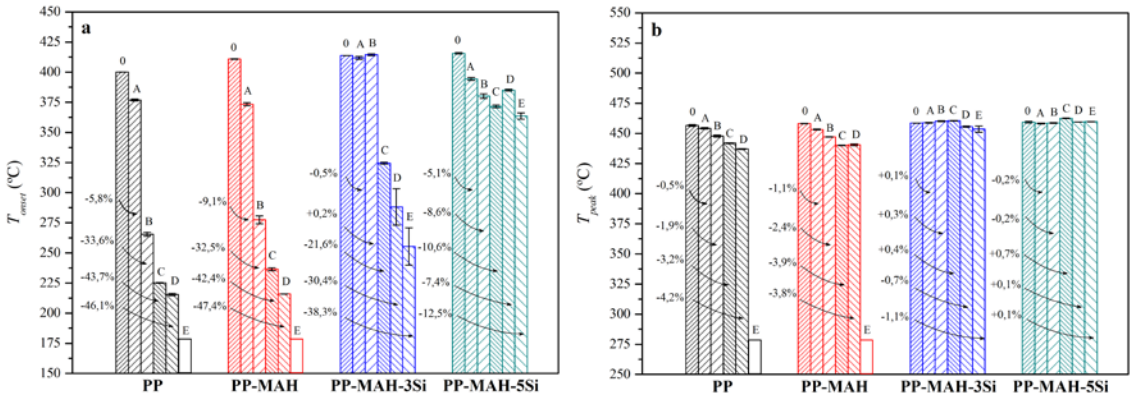

Figure 13. Thermal decomposition onset (a) and peak (b) temperatures (T_{onset} and T_{peak}) for raw PP, PP-MAH and PP-MAH-Si composites irradiated in the UV-visible wavelength range (λ = 280 – 800 nm) (Stages: A = 250 h; B = 750 h; C = 1500 h; D = 2250 h; E = 3000 h).

4. Conclusions

This paper shows the potential of novel patented high-tech silicon microparticles to protect polypropylene from degradation during both processing and accelerated sunlight irradiation. Silicon colloids provided UV-protection which hindered the chemi-crystallisation phenomenon. Preservation of appearance, thermal, structural and mechanical properties as well as thermal decomposition behaviour were found. The stabilization of PP was more relevant for samples loaded with 5 wt% of Si.

The addition of silicon microparticles to coupled raw polypropylene matrix did not significantly alter the thermal processing conditions. It just slightly reduced the time of crystallization upon cooling and offered similar crystalline populations, with close lamellar thickness distributions, regardless the amount of Si microparticles. Similar thermal decomposition profiles were also found. Finally, mechanical properties were affected by increasing the dynamic storage modulus up to a 115 %, result which was independent form the nucleation effect of Si to grow crystal fractions in the PP matrix.

Acknowledgements

B.Sc. A. Montesinos is acknowledged for his dedication in the lab and his outstanding attitude towards learning. Ph.D. L. Santonja-Blasco is thanked for revision of the work and endless and enjoyable discussions. The authors would like to acknowledge the Spanish Ministry of Economy and Competitiveness, through the Research Project MAT2012-3504. The Spanish Ministry of Education, Culture and Sports is also thanked for the predoctoral FPU grant of O. Gil-Castell (FPU13/01916). Generalitat Valenciana is thanked for the PROMETEOII/2014/026, the APOSTD 2014/041 of J.D. Badia and the GRISOLIA/2012/003 for R. Teruel-Juanes. Universitat Politècnica de València is thanked for the support through the PAID-06-SP20120581 project and for the FPI grant of O. Gil-Castell. Repsol (Tarragona, Spain) is acknowledged for providing the raw polypropylene (PP) homopolymer.

References

[1] Maier C, Haber T. Polypropylene. The Definitive User's Guide and Databook. Norwich: William Andrew; 1998. ISBN: 978-1-884207-58-7.

[2] Carlsson DJ, Wiles DM. The photo-oxidation of polypropylene. Part I. Photooxidation and photoinitiation processes. Journal of Macromolecular Science - Reviews in Macromolecular Chemistry & Physics 1976;14:65-106.

[3] Rabek JF. Photostabilization of polymers. London and New York: Elsevier Applied Science; 1990.

[4] Quin H, Zhang S, Liu H, Xie S, Yang M, Shen D. Photo-oxidative degradation of polypropylene/montmorillonite nanocomposites. Polymer 2005;46(9)3149-3156.

[5] Morlat S, Mailhot B, Gonzalez D, Gardette JL. Photo-oxidation of PP/montmorillonite nanocomposites. Influence of nanoclay and compatibilizing agent. Chemistry of Materials 2004;16:377-383.

[6] Carlsson DJ , Garton A , Wiles DM. Initiation of Polypropylene Photooxidation. 2. Potential Processes and Their Relevance to Stability. Macromolecules 1976;9(5)695-701.

[7] Gugumus F. In: Scott G, editor. Developments in polymer stabilisation – 1. London: Applied Science Publishers Ltd.; 1979.

[8] Gugumus F. Possibilities and limits of synergism with light stabilizers in polyolefins: 1. HALS in polyolefins. Polymer Degradation and Stability, 2002; 75: 295-308.

[9] Gijsman P. Polymer Stabilization. Handbook of Environmental Degradation of Materials. Oxford: Elsevier; 2012.

[10] Carlsson DJ, Zhang K, Wiles DM. Polypropylene photostabilization by hindered amines in the presence of acidic species. Journal of Applied Polymer Science 1987;33:875-84.

[11] Saenz de Juano V. Contribución al estudio de la degradación ambiental de poliolefinas fotoestabilizadas. PhD Thesis. Universitat Politècnica de València: Spain.

[12] Gugumus F. In: Klemchuk P, Pospisil J, editors. Inhibition of oxidation processes in organic materials, vol. 2. Boca Raton, Florida (USA): CRC Press; 1989.

[13] Gugumus F, Zweifel H, editors. Plastics additives handbook, 5th edition, Munich: Hanser Publishers; 2001.

[14] Ammala A, Hill AJ, Meakin P, Pas SJ, Turney TW. Degradation studies of polyolefins incorporating nanoparticulate zinc oxide UV stabilizers. Journal of Nanoparticle Research 2002;4:167-174.

[15] Zhao H, Robert K. Y. Li. A study on the photo-degradation of zinc oxide (ZnO) filled polypropylene composites. Polymer 2006;47:3207-3217.

[16] Allen NS, Chirinis-Padron A, Henman TJ. The photo-stabilisation of polypropylene: A review. Polymer Degradation and Stability 1985;13:31-76.

[17] Li R, Yabe S, Yamashita M, Momose S, Yoshida S, Yin S, Sato T. UV-shielding properties of zinc oxide-doped ceria fine powders derived via soft solution chemical routes. Materials Chemistry and Physics 2002;75:39-44.

[18] Moustaghfir A, Rivaton A, Tomasella E, Mailhot B, Cellier J, Jacquet M, Gardette JL. Photostabilization of polycarbonate by ZnO coatings. Journal of Applied Polymer Science 2004;95(2):380-385.

[19] Reijnders L. The release of TiO2 and SiO2 nanoparticles from composites. Polymer Degradation and Stability 2009; 94(5):873-876.

[20] Fenollosa R, Meseguer F, Tymczenko M. Silicon Colloids: From Microcavities to Photonic Sponges. Advanced Materials 2008;20(1):95-98.

[21] Fenollosa R, Meseguer F, Tymczenko M. Spain patent no. PCT/ES2008/070102 (18 June 2007).

[22] Fenollosa R, Meseguer F, Tymczenko M. U. S. Patent no. 11/984870 (23 November 2007).

[23] I. Rodriguez, R. Fenollosa, F. Meseguer, A. Perez-Roldan. Patent Ref. WO 2012/101306. Formulation comprising silicon microparticles, as a pigment that can absorb visible, UV radiation and reflect IR radiation.

[24] Holsti-Miettinen R, Seppala J, Ikkala OT. Effects of compatibilizers on the properties of polyamide/polypropylene blends. Polymer Engineering & Science 1992;32(13):868-877.

[25] Cho K, Li F, Choi J. Crystallization and melting behaviour of polypropylene and maleated polypropylene blends. Polymer 1999;40:1719-1729.

[26] Morreale M, Dintcheva N Tz, La Mantia FP. Accelerated weathering of PP based nanocomposites: Effect of the presence of maleic anhydride grafted polypropylene. eXPRESS Polymer Letters 2013;7(8):703-715.

[27] Mailhot B, Morlat S, Gardette JL, Boucard S, Duchet J, Gérard JF. Photodegradation of polypropylene nanocomposites. Polymer Degradation and Stability 2003;82:163-167.

[28] García-López D, Picazo O, Merino JC, Pastor JM. Polypropylene-clay nanocomposites: effect of compatibilizing agents on clay dispersión. European Polymer Journal 2003;39(5):945-950.

[29] Xu W, Liang G, Zhai H, Tang S, Hang G, Pan WP. Preparation and crystallization behavior of PP/PP-g-MAH/Org-MMT nanocomposite. European Polymer Journal 2003;39(7):1467-1474.

[30] Rong MZ, Zhang MQ, Ruan WH. Surface modification of nanoscale fillers for improving properties of polymer nanocomposites: a review. Materials Science and Technology 2006;22(7):787-796.

[31] Chen XM, Shen JW, Huang WY. Novel electrically conductive polypropylene/graphite nanocomposites. Journal of Materials Science Letters 2002;21(3):213-214.

[32] Ray S, Okamoto M. Polymer/layered silicate nanocomposites: a review from preparation to processing. Progress in Polymer Science 2003;28:1539–641.

[33] Paul DR, Robeson LM. Polymer nanotechnology: nanocomposites. Polymer 2008;49:3187–3204.

[34] Usuki A, Kojima Y, Kawasumi M, Okada A, Fukusihima Y, Kurauchi TT. Synthesis of nylon 6-clay hybrid. Material Research 1993;8:1179–1184.

[35] Palza H, Reznik B, Kappes M, Hennrich F, Naue IFC, Wilhelm M. Characterization of melt flow instabilities in polyethylene/carbon nanotube composites. Polymer 2010;51:3753–3761.

[36] Robinson J, Poulsen KV, Högström PA, Linder A, Burkhard H, Kobilsek M, Gemmel A. Comparison of standard UV tests methods for the ageing of cables. Proceedings of the 60th IWCS Conference. International Wire & Cable Symposium, 2011; pp. 329-337.

[37] Wunderlich B, Thermal Analysis, London: Academic Press; 1990.

[38] Lauritzen JL, Hoffman JD. Theory of formation of polymer crystals with folded chains in dilute solution. Journal of Research of the National Bureau of Standards 1960;64:73-102.

[39] Lauritzen JL, Hoffman JD. Crystallization of bulk polymers with chain folding: theory of growth of lamellar spherulites. Journal of Research of the National Bureau of Standards 1961;65:297-336.

[40] Hoffman JD, Davis GT, Lauritzen JL. In: Hannay NB, editor. Crystalline and noncrystalline solids, vol. 3. New York: Plenum Press; 1976.

[41] Mark James E. Polymer Data Handbook, New York: Oxford University Press; 1999.

[42] Samuels RJ. Quantitative structural characterization of the melting behavior of isotactic polypropylene. Journal of Polymer Scence 1975;13:1417.

[43] Guerra G, Petraccone V, Corradini P, De-Rosa C, Napolitano R, Pirozzi B, Giunchi G. Crystalline order and melting behavior of isotactic polypropylene (α form). Journal of Polymer Science, Polymer Physics 1984;22:1029.

[44] Rabello MS, White JR. Photodegradation of polypropylene containing a nucleating agent. Journal of Applied Polymer Science 1997;64(13):2505-2517.

[45] Tang J, Wang Y, Liu H, Belfiore A. Effects of organic nucleating agents and zinc oxide nanoparticles on isotactic polypropylene crystallization. Polymer 2004;45:2081-2091.

[46] Chen X, Yu J, Guo S. Structure and properties of polypropylene composites filled with magnesium hydroxide. Journal of Applied Polymer Science 2006;102:4943-4951.

[47] Ming-Rui M, Qiang D. Effect of filler treatment on crystallization morphology and mechanical properties of polypropylene/calcium carbonate composites. Journal of Macromolecular Science, Part B: Physics 2009;48:213-225.

[48] Palza H, Vergara R, Zapata P. Composites of polypropylene melt blended with synthesized silica nanoparticles. Composites Science and Technology 2011;71:535-540.

[49] Sternstein SS, Zhu AJ. Reinforcement mechanism of nanofilled polymer melts as elucidated by nonlinear viscoelastic behaviour. Macromolecules 2002;35:7262-7273.

[50] Manias E. Nanocomposites – Stiffer by design. Nature Materials 2007;6:9-11.

[51] Rabello MS, White JR. Crystallization and melting behaviour of photodegraded polypropylene – I. Chemi-crystallization. Polymer 1997; 38(26):6379-6387.

[52] Papet G, Jirackova-Audouin L, Verdu J. Diffusion controlled radiochemical oxidation of low density polyethylene-I. Depth dependence of morphological changes. Radiation Physics and Chemistry 1987;29:65-69.

[53] Wunderlich B. Macromolecular Physics. Vol. 2: Crystal Nucleation, Growth, Annealing, New York: Academic Press; 1976.

[54] Schoolenberg GE, Vink P. Ultra-violet degradation of polypropylene: 1. Degradation profile and thickness of the embrittled surface layer. Polymer 1991;32:432-437.

[55] Schoolenberg GE, Meijer HDF. Ultra-violet degradation of polypropylene: 2. Residual strength and failure mode in relation to the degraded surface layer. Polymer 1991;32:438-444.

[56] Badía JD, Vilaplana F, Karlsson S, Ribes-Greus A. Thermal analysis as a quality tool for assessing the influence of thermo-mechanical degradation on recycled poly(ethylene terephthalate). Polymer Testing 2009; 28(2):169-75.

[57] Rabello MS, White JR. Crystallization and melting behaviour of photodegraded polypropylene – II. Re-crystallization of degraded molecules. Polymer 1997; 38(26):6389-6399.

[58] Martuscelli E, Pracella M, Crispino L. Crystallization behaviour of fractions of isotactic polypropylene with different degrees of stereoregularity. Polymer 1983;24(6):693-699.

[59] Janimak JJ, Cheng SZD, Giusti PA, Hsieh ET. Isotacticity effect on crystallization and melting in polypropylene fractions. II. Linear crystal growth rate and morphology study. Macromolecules 1991;24(9):2253–2260..

[60] Kamide K, Yamaguchi K. Change in fine structures of isotactic polpropylene during isothermal crystallization. Die Makromolekulare Chemie 1972;162(1)219-233.

[61] Shi G, Zhang X, Cao Y, Hong J. Melting behavior and crystalline order of ß-crystalline phase poly(propylene). Die Makromolekulare Chemie 1993; 149(1)269-277.

[62] Rybnikar FJ. Transition of β to α phase in isotactic polypropylene. Journal of Macromolecular Science – Physics 1991;30(3)201-223.

[63] O'Kane WJ, Young RJ, Ryan AJ, Bras W, Derbyshire GE, Mant GR. Simultaneous SAXS/WAXS and DSC analysis of the melting and recrystallization behaviour of quenched polypropylene. Polymer 1994;35(7):1352-1358.

[64] Janimak JJ, Cheng SZD, Zhang A, Hsieh ET. Isotacticity effect on crystallization and melting in polypropylene fractions: 3. Overall crystallization and melting behaviour. Polymer 1992; 33(4);728-735.

[65] Duvall J, Selliti C, Myers C, Hiltner A, Baer E. Interfacial effects produced by crystallization of polypropylene with polypropylene-g-maleic anhydride compatibilitzers. Journal of Applied Polymer science 1994;52(2)207-216.

[66] Badia JD, Santonja-Blasco L, Martínez-Felipe A, Ribes-Greus A. Hygrothermal ageing of reprocessed polylactide. Polymer Degradatio and Stability 2012;97(10):1881-1890.

[67] Badia JD, Strömberg E, Karlsson S, Ribes-Greus A. Material valorisation of amorphous polylactide. influence of thermo-mechanical degradation on the morphology, segmental dynamics, thermal and mechanical performance. Polymer Degradation and Stability 2012, 97(4):670-678.

[68] Badia JD, Strömberg E, Karlsson S, Ribes-Greus A. The role of crystalline, mobile amorphous and rigid amorphous fractions in the performance of recycled poly (ethylene terephthalate) (PET). Polymer Degradation and Stability 2012;97(1):98-107.

[69] Santonja-Blasco L, Moriana R, Badía JD, Ribes-Greus A. Thermal analysis applied to the characterization of degradation in soil of polylactide: I. calorimetric and viscoelastic analyses. Polymer Degradation and Stability 2010;95(11):2192-2199.

[70] Santonja-Blasco L, Ribes-Greus A, Alamo RG. Comparative thermal, biological and photodegradation kinetics of polylactide and effect on crystallization rates. Polymer Degradation and Stability 2013;98(3):771-784.

[71] Blais P, Carlsson DJ, Wiles DM. Surface changes during polypropylene photo-oxidation: A study by infrared spectroscopy and electron microscopy. Journal of Polymer Science Part A-1: Polymer Chemistry 1972;10:1077-1092.

[72] Vink P. Degradation and Stabilisation of Polyolefins, ed. N.S. Allen. London: Applied Science; 1983.

[73] Severini F, Gallo R, Ipsale S. Environmental degradation of polypropylene. Polymer Degradation and Stability 1988;22:185-194.

[74] Mani R, Singh RP, Sivaram S, Lacoste J. Effect of UV irradiation on the structure of heterophasic ethylene-propylene copolymers. Polymer Journal 1994;26(10):1132-1141.

[75] Ogier L, Rabello MS, White JR. Influence of morphology and surface preparation on the weatherability of polypropylene. Journal of Materials Science 1995; 30(9):2364-2376.

[76] Rabello MS, White JR. Photodegradation of talc-filled polypropylene. Polymer composites 1996;17:691-704.

[77] Rabello MS, White JR. The role of physical structure and morphology in the photodegradation behaviour of polypropylene. Polymer Degradation and Stability 1997;56:55-73.

[78] Bohren CF and Huffman DR, Absorption and Scattering of Light by Small Particles. John Wiley & Sons, New York, 1998.

[79] Badia JD, Martinez-Felipe A, Santonja-Blasco L, Ribes-Greus A. Thermal and thermo-oxidative stability of reprocessed poly(ethylene terephthalate). Journal Analytical of Applied Pyrolysis 2013;99:191-202.

[80] Badia JD, Santonja-Blasco L, Martínez-Felipe A, Ribes-Greus A. Reprocessed polylactide: Studies of thermo-oxidative decomposition. Bioresource Technology 2012;114:622-8.

[81] Badia JD, Santonja-Blasco L, Martínez-Felipe A, Ribes-Greus A. A methodology to assess the energetic valorization of bio-based polymers from the packaging industry: Pyrolysis of reprocessed polylactide. Bioresource Technology 2012;111:468-475.

ANNEX – OPEN ACCESS POLICIES

SHERPA/RoMEO

. . . opening access to research

Home • Search • Journals • Publishers • FAQ • Suggest • About

English | Español | Magyar | Nederlands | Português

Search - Publisher copyright policies & self-archiving

One journal found when searched for: **european polymer journal**

Journal:	European Polymer Journal (ISSN: 0014-3057, ESSN: 1873-1945)
RoMEO:	This is a RoMEO green journal
Paid OA:	A paid open access option is available for this journal.
Author's Pre-print:	✓ author can archive pre-print (ie pre-refereeing)
Author's Post-print:	✓ author can archive post-print (ie final draft post-refereeing)
Publisher's Version/PDF:	✗ author cannot archive publisher's version/PDF
General Conditions:	• Author: pre-print on any website, including arXiv and RePEC • Author's post-print on author's personal website immediately • Author's post-print on open access repository after an embargo period of between 12 months and 48 months • Permitted deposit due to Funding Body, Institutional and Governmental policy or mandate, may be required to comply with embargo periods of 12 months to 48 months • Author's post-print may be used to update arXiv and RepEC • Publisher's version/PDF cannot be used • Must link to publisher version with DOI • Author's post-print must be released with a Creative Commons Attribution Non-Commercial No Derivatives License
Mandated OA:	Compliance data is available for 57 funders
Paid Open Access:	Open Access
Notes:	• Publisher last reviewed on 03/06/2015
Copyright:	Unleashing the power of academic sharing - Sharing Policy - Sharing and Hosting Policy FAQ - Green open access - Journal Embargo Period List (pdf) - Journal Embargo List for UK Authors Attaching a User License (pdf) - Funding Body Agreements
Updated:	01-May-2015 - Suggest an update for this record
Link to this page:	http://www.sherpa.ac.uk/romeo/issn/0014-3057/
Published by:	Elsevier - Green Policies in RoMEO

This summary is for the journal's default policies, and changes or exceptions can often be negotiated by authors.
All information is correct to the best of our knowledge but should not be relied upon for legal advice.